

## Intermolecular Alignment in $\beta_2$ -Microglobulin Amyloid Fibrils

Galia T. Debelouchina,<sup>†</sup> Geoffrey W. Platt,<sup>‡</sup> Marvin J. Bayro,<sup>†</sup> Sheena E. Radford,<sup>‡</sup> and Robert G. Griffin<sup>\*†</sup>

Department of Chemistry and Francis Bitter Magnet Laboratory, Massachusetts Institute of Technology, Cambridge, Massachusetts 02139, United States, and Astbury Centre for Structural Molecular Biology and Institute of Molecular and Cellular Biology, University of Leeds, Leeds LS2 9JT, U.K.

Received September 4, 2010; E-mail: rgg@mit.edu

**Abstract:** The deposition of amyloid-like fibrils, composed primarily of the 99-residue protein  $\beta_2$ -microglobulin ( $\beta_2m$ ), is one of the characteristic symptoms of dialysis-related amyloidosis. Fibrils formed *in vitro* at low pH and low salt concentration share many properties with the disease related fibrils and have been extensively studied by a number of biochemical and biophysical methods. These fibrils contain a significant  $\beta$ -sheet core and have a complex cryoEM electron density profile. Here, we investigate the intrasheet arrangement of the fibrils by means of  $^{15}N$ - $^{13}C$  MAS NMR correlation spectroscopy. We utilize a fibril sample grown from a 50:50 mixture of  $^{15}N$ ,  $^{12}C$ - and  $^{14}N$ ,  $^{13}C$ -labeled  $\beta_2m$  monomers, the latter prepared using 2- $^{13}C$  glycerol as the carbon source. Together with the use of ZF-TEDOR mixing, this sample allowed us to observe intermolecular  $^{15}N$ - $^{13}C$  backbone-to-backbone contacts with excellent resolution and good sensitivity. The results are consistent with a parallel, in-register arrangement of the protein subunits in the fibrils and suggest that a significant structural reorganization occurs from the native to the fibril state.

$\beta_2$ -Microglobulin ( $\beta_2m$ ) is a 99-residue protein that forms amyloid fibril deposits associated with dialysis-related amyloidosis (DRA).<sup>1</sup> Under acidic conditions (pH = 2.5) and low salt concentration, the protein can also form amyloid fibrils *in vitro* through a nucleation-dependent mechanism.<sup>2,3</sup> These fibrils are long, straight, and unbranched in appearance (Figure S1) and share many properties with the fibrils isolated from tissues of DRA patients, including the same characteristic amide I' band in FTIR spectra.<sup>4</sup> It has been shown that the fibrils themselves, and not the prefibrillar oligomeric species formed in the lag phase of assembly, can disrupt model membranes and are toxic to cells.<sup>5</sup> While an atomic structural model for these fibrils is not yet available, structural details emerged first through methods like limited proteolysis,<sup>6,7</sup> hydrogen exchange,<sup>8,9</sup> and more recently by magic angle spinning (MAS) NMR,<sup>10</sup> electron paramagnetic resonance (EPR),<sup>11</sup> and cryo-electron microscopy (cryoEM).<sup>12</sup> In particular, analysis of the chemical shifts of 64 assigned residues of  $\beta_2m$  fibrils has shown that the protein contains a rigid fibril core with substantially more  $\beta$ -sheet character than the native protein.<sup>10</sup> CryoEM maps revealed a complex picture of the fibrils, where non-native globular  $\beta_2m$  monomers pack in "dimer-of-dimers" building blocks that associate asymmetrically into crescent-shaped units.<sup>12</sup> In addition, site-directed EPR spin labeling suggested that the major building block consists of six  $\beta_2m$  polypeptide chains, arranged in a parallel, in-register manner.<sup>11</sup>

In the experiments described here, we investigate the tertiary structure of  $\beta_2m$  amyloid fibrils with  $^{15}N$ - $^{13}C$  MAS NMR correla-

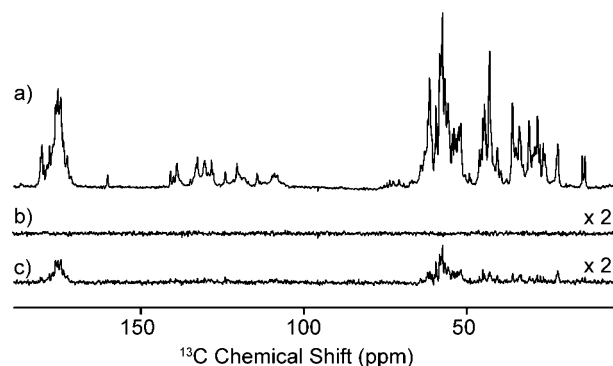


**Figure 1.** (a)  $^{13}C$  CP spectrum of mixed 2- $\beta_2m$  fibrils, 512 scans; (b) ZF-TEDOR spectrum obtained with  $\tau_{mix} = 1.76$  ms, 512 scans; (c) ZF-TEDOR with  $\tau_{mix} = 18$  ms, 5120 scans.

tion spectroscopy. MAS NMR has been successfully used to obtain information about the inter- and intramolecular interactions that form the  $\beta$ -sheet core of amyloid fibrils, including  $A\beta(1-40)$ ,<sup>13</sup> a 22-residue fragment of  $\beta_2m$ ,<sup>14</sup> Het-s(218-289),<sup>15</sup> and curli amyloid.<sup>16</sup> Various sample preparation techniques and experiments have been employed to achieve that end, including methods that rely on the incorporation of single labels<sup>17,18</sup> or proton-mediated transfer.<sup>19</sup> Here, we use ZF-TEDOR (z-filtered transferred echo double resonance) mixing<sup>20,21</sup> to obtain intermolecular  $^{15}N$ - $^{13}C$  correlations that establish that the protein subunits in long, straight  $\beta_2m$  fibrils formed at pH 2.5 are arranged as parallel, in-register  $\beta$ -sheets.

Our experiments utilize fibrils formed from a 50:50 mixture of  $^{15}N$ ,  $^{12}C$ - and  $^{14}N$ ,  $^{13}C$ -labeled  $\beta_2m$  monomers, the latter half being prepared using [2- $^{13}C$ ]-glycerol as the carbon source. This sample, referred to as "mixed 2- $\beta_2m$ ", offers improved resolution in the  $^{13}C$  dimension<sup>22-24</sup> (Figure 1a) as well as potential gains in experimental transfer efficiency due to the significantly reduced number of directly bonded  $^{13}C$  atoms.<sup>25</sup> The absence of  $^{13}C$   $J$ -couplings and the elimination of strong (intramolecular) dipolar  $^{15}N$ - $^{13}C$  couplings as a result of the mixed nature of the sample improve the efficiency of ZF-TEDOR.<sup>20,26,27</sup>

In a 100% uniformly  $^{15}N$ ,  $^{13}C$  labeled  $\beta_2m$  sample, the experimental one-bond  $^{15}N$ - $^{13}C$  transfer efficiency after 1.76 ms of ZF-TEDOR mixing is typically  $\sim 20\%$  of the  $^{13}C$  CP signal. In the mixed 2- $\beta_2m$  sample, after such a short mixing time, no significant buildup of  $^{13}C$  polarization is observed, as shown in Figure 1b. This is due to the absence of  $^{13}C$  nuclei in the  $^{15}N$ ,  $^{12}C$ -labeled monomers, which were prepared using  $^{13}C$ -depleted glucose (99.9% purity) to eliminate contributions from natural abundance. In particular, signals from one-bond  $^{15}N$ - $^{13}C$  interactions are not detected. On the other hand, longer ZF-TEDOR mixing times lead to the buildup of  $^{13}C$  intensity, which reaches a maximum at 18 ms (Figure 1c and Figure S2) and is consistent with  $^{15}N$ - $^{13}C$

<sup>†</sup> Francis Bitter Magnet Laboratory and Massachusetts Institute of Technology.

<sup>‡</sup> Astbury Centre for Structural Molecular Biology and University of Leeds.

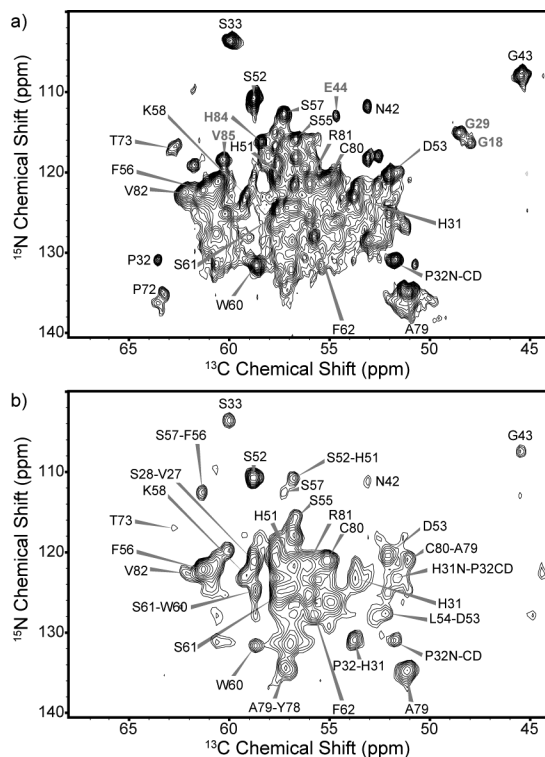


**Figure 2.** Comparison of the  $^{15}\text{N}$ – $^{13}\text{C}\alpha$  region of correlation spectra obtained with ZF-TEDOR mixing for two differently labeled  $\beta_2\text{m}$  fibril samples. (a)  $2\text{-}\beta_2\text{m}$ ,  $\tau_{\text{mix}} = 1.6$  ms, 12 mg of sample, 2 days of experimental time. Labels correspond to intramolecular  $\text{N}_i\text{-C}\alpha_i$  transfer, unless otherwise noted, while labels in gray denote cross-peaks that appear only in the  $2\text{-}\beta_2\text{m}$  spectrum. (b) Mixed  $2\text{-}\beta_2\text{m}$ ,  $\tau_{\text{mix}} = 16$  ms, 16 mg of sample, 9 days of experimental time. Labels correspond to intermolecular  $\text{N}_i\text{-C}\alpha_i$  or  $\text{N}_i\text{-C}\alpha_{i-1}$  transfer, unless otherwise noted.

distances of  $\sim 5.0\text{--}5.5$  Å. The maximum bulk transfer efficiency for the  $\text{C}\alpha$  region is  $\sim 3\%$ , which is better than the experimental transfer efficiencies observed for uniformly  $^{13}\text{C}$  labeled samples ( $<1\%$  for similar distances).<sup>20</sup>

In order to obtain site-specific information regarding the origin of the  $^{15}\text{N}$ – $^{13}\text{C}$  intermolecular contacts in mixed  $2\text{-}\beta_2\text{m}$ , we recorded a 2D ZF-TEDOR experiment with  $\tau_{\text{mix}} = 16$  ms (Figure S3). This spectrum presents excellent resolution ( $^{13}\text{C}$  line widths  $\sim 50$  Hz) and sufficient sensitivity after a long acquisition period, which was facilitated by the robustness of the TEDOR sequence. Overall, the positions of the observed cross-peaks in this mixed  $2\text{-}\beta_2\text{m}$  spectrum correspond exactly with the positions of cross-peaks in one-bond (Figure 2a) or two-bond TEDOR spectra (data not shown) of a  $\beta_2\text{m}$  fibril sample prepared from 100%  $^{15}\text{N}$ ,  $2\text{-}^{13}\text{C}$  glycerol labeled material ( $2\text{-}\beta_2\text{m}$ ). The majority of the cross-peaks in the mixed  $2\text{-}\beta_2\text{m}$  sample could be readily assigned based on known chemical shifts of long, straight  $\beta_2\text{m}$  fibrils,<sup>10</sup> and they correspond exclusively to intermolecular  $\text{N}_i\text{-C}\alpha_i$ ,  $\text{N}_i\text{-C}\alpha_{i-1}$ ,  $\text{N}_i\text{-CO}_i$ , or  $\text{N}_i\text{-CO}_{i-1}$  transfer (Figures 2b and S3). In particular, the following residues giving rise to intermolecular contacts in the mixed  $2\text{-}\beta_2\text{m}$  sample were assigned: H31–S33, N42, G43, R45, I46, V49, H51–F62, P72, T73, and Y78–V82. While P32, S33, G43, F56, S57, K58, and F62 are part of well-ordered loops in the fibrils, the remainder of the residues represent all of the currently assigned fibril  $\beta$ -strands.

Some cross-peaks in Figure 2b (mixed  $2\text{-}\beta_2\text{m}$ ) do not presently have assignments. Conversely, not all of the strong cross-peaks shown in Figure 2a ( $2\text{-}\beta_2\text{m}$ ) appear in the mixed  $2\text{-}\beta_2\text{m}$  spectrum. This includes G18, G29, E44, H84, and V85 (shown in gray in Figure 2a) among others. This is most likely due to differences in

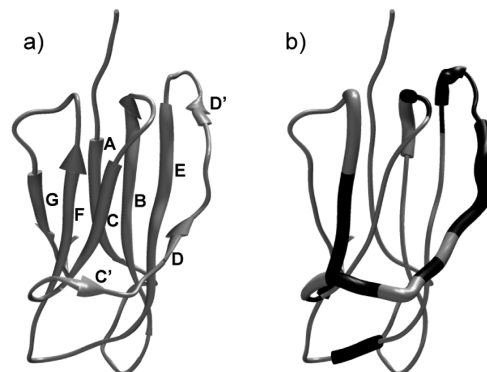


**Figure 3.** (a) Crystal structure of native monomeric  $\beta_2\text{m}$  (PDB ID: 1DUZ)<sup>28</sup> showing the antiparallel  $\beta$ -sheet arrangement of the strands (labeled A to G). (b) Residues that form  $\beta$ -strands in fibrillar  $\beta_2\text{m}$  painted onto the native fold.  $\beta$ -Strands in the fibrils<sup>10</sup> are shown as thick tubes, and the residues giving rise to assigned intermolecular  $\text{N}_i\text{-C}\alpha_i$  cross-peaks are shown in black. The structures were prepared using the Chimera software.<sup>29</sup>

local dynamics and relaxation whose effects are exacerbated at long mixing times, resulting in large variations in the cross-peak intensities.<sup>30</sup>

The data presented above suggest that long, straight  $\beta_2\text{m}$  fibrils grown at pH 2.5 and low salt concentration form parallel, in-register  $\beta$ -sheets. In such a case the average distances for intermolecular  $\text{N}_i\text{-C}\alpha_i$  and  $\text{N}_i\text{-C}\alpha_{i-1}$  contacts are  $\sim 5$  and  $\sim 5.5$  Å respectively (Figure S4), which is consistent with the bulk ZF-TEDOR buildup (Figure S2). In order to accommodate such an arrangement, substantial reorganization of the native antiparallel  $\beta$ -sheet structure<sup>31–33</sup> is required, indicating that the structure of the monomers within the fibrils must be highly non-native. Figure 3 highlights two clear pieces of evidence for the non-native structure of  $\beta_2\text{m}$  within fibrils: first, residues involved in loops/turns in native  $\beta_2\text{m}$  (Figure 3a) reorganize to form ordered  $\beta$ -strands in the fibrils (Figures 3b and S5), and second, while all  $\beta$ -strands form antiparallel  $\beta$ -sheet contacts with residues distant in sequence in native  $\beta_2\text{m}$ ,  $\beta$ -strands in the fibrils are parallel and in register.

The parallel arrangement of the  $\beta$ -strands in  $\beta_2\text{m}$  fibrils was predicted initially by FTIR experiments<sup>34,35</sup> and is in agreement with data obtained by site-directed spin labeling and EPR.<sup>11</sup> The results described here verify and expand upon the latter, which indicates that spin labels attached to cysteine-substituted residues S33, S55, S61, and T73 among others give EPR spectra indicative of immobile, parallel, and in-register stacked spin labels (Figure S5). Stacks of six  $\beta_2\text{m}$  monomers arranged in that manner are then required to fulfill the electron density maps obtained by cryoEM.<sup>12</sup> The site-specific information regarding the intermolecular arrangement of  $\beta_2\text{m}$  fibrils presented here provides an important step toward a full molecular model of the fibrils. Additional experiments, particularly aimed at determining the quaternary fold of the fibrils, are in progress and should shed light on how this tertiary fibril arrangement fits into such a complex cryoEM electron density profile.

**Acknowledgment.** The authors would like to acknowledge financial support from NIH Grants EB003151 and EB002026 and the Wellcome Trust (Grant Numbers 075675 and 062164). We thank Dr. Kendra Frederick for helpful discussions and suggestions. Molecular graphic images were produced using the UCSF Chimera package from the Resource for Biocomputing, Visualization, and Informatics at the University of California, San Francisco (supported by NIH P41 RR-01081).

**Supporting Information Available:** Sample and experimental details; EM image of the fibrils; 1D ZF-TEDOR buildup; full 2D ZF-TEDOR spectrum; expected intermolecular distances in a parallel, in-register arrangement; summary of the available sequence-specific structural information for the fibrils. This material is available free of charge via the Internet at <http://pubs.acs.org>.

## References

- (1) Gejyo, F.; Yamada, T.; Odani, S.; Nakagawa, Y.; Arakawa, M.; Kunitomo, T.; Kataoka, H.; Suzuki, M.; Hirasawa, Y.; Shirahama, T.; Cohen, A. S.; Schmid, K. *Biochem. Biophys. Res. Commun.* **1985**, *129*, 701–706.
- (2) Platt, G. W.; Radford, S. E. *FEBS Lett.* **2009**, *583*, 2623–2629.
- (3) Xue, W. F.; Homans, S. W.; Radford, S. E. *Proc. Natl. Acad. Sci. U.S.A.* **2008**, *105*, 8926–8931.
- (4) Jahn, T. R.; Tennent, G. A.; Radford, S. E. *J. Biol. Chem.* **2008**, *283*, 17279–17286.
- (5) Xue, W. F.; Hellewell, A. L.; Gosal, W. S.; Homans, S. W.; Hewitt, E. W.; Radford, S. E. *J. Biol. Chem.* **2009**, *284*, 34272–34282.
- (6) Monti, M.; Amoresano, A.; Giorgetti, S.; Bellotti, V.; Pucci, P. *Biochim. Biophys. Acta, Proteins Proteomics* **2005**, *1753*, 44–50.
- (7) Myers, S. L.; Thomson, N. H.; Radford, S. E.; Ashcroft, A. E. *Rapid Commun. Mass Spectrom.* **2006**, *20*, 1628–1636.
- (8) Hoshino, M.; Katou, H.; Hagihara, Y.; Hasegawa, K.; Naiki, H.; Goto, Y. *Nat. Struct. Biol.* **2002**, *9*, 332–336.
- (9) Yamaguchi, K. I.; Katou, H.; Hoshino, M.; Hasegawa, K.; Naiki, H.; Goto, Y. *J. Mol. Biol.* **2004**, *338*, 559–571.
- (10) Debelouchina, G. T.; Platt, G. W.; Bayro, M. J.; Radford, S. E.; Griffin, R. G. *J. Am. Chem. Soc.* **2010**, *132*, 10414–10423.
- (11) Ladner, C. L.; Chen, M.; Smith, D. P.; Platt, G. W.; Radford, S. E.; Langen, R. *J. Biol. Chem.* **2010**, *285*, 17137–17147.
- (12) White, H. E.; Hodgkinson, J. L.; Jahn, T. R.; Cohen-Krausz, S.; Gosal, W. S.; Muller, S.; Orlova, E. V.; Radford, S. E.; Saibil, H. R. *J. Mol. Biol.* **2009**, *389*, 48–57.
- (13) Petkova, A. T.; Ishii, Y.; Balbach, J. J.; Antzutkin, O. N.; Leapman, R. D.; Delaglio, F.; Tycko, R. *Proc. Natl. Acad. Sci. U.S.A.* **2002**, *99*, 16742–16747.
- (14) Iwata, K.; Fujiwara, T.; Matsuki, Y.; Akutsu, H.; Takahashi, S.; Naiki, H.; Goto, Y. *Proc. Natl. Acad. Sci. U.S.A.* **2006**, *103*, 18119–18124.
- (15) Wasmer, C.; Lange, A.; Van Melckebeke, H.; Siemer, A. B.; Riek, R.; Meier, B. H. *Science* **2008**, *319*, 1523–1526.
- (16) Shewmaker, F.; McGlinchey, R. P.; Thurber, K. R.; McPhie, P.; Dyda, F.; Tycko, R.; Wickner, R. B. *J. Biol. Chem.* **2009**, *284*, 25065–25076.
- (17) Tycko, R. *J. Chem. Phys.* **2007**, *126*, 9.
- (18) Benzinger, T. L. S.; Gregory, D. M.; Burkoth, T. S.; Miller-Auer, H.; Lynn, D. G.; Botto, R. E.; Meredith, S. C. *Proc. Natl. Acad. Sci. U.S.A.* **1998**, *95*, 13407–13412.
- (19) Lange, A.; Luca, S.; Baldus, M. *J. Am. Chem. Soc.* **2002**, *124*, 9704–9705.
- (20) Jaroniec, C. P.; Filip, C.; Griffin, R. G. *J. Am. Chem. Soc.* **2002**, *124*, 10728–10742.
- (21) Hing, A. W.; Vega, S.; Schaefer, J. J. *Magn. Reson.* **1992**, *96*, 205–209.
- (22) LeMaster, D. M.; Kushlan, D. M. *J. Am. Chem. Soc.* **1996**, *118*, 9255–9264.
- (23) Castellani, F.; van Rossum, B.; Diehl, A.; Schubert, M.; Rehbein, K.; Oschkinat, H. *Nature* **2002**, *420*, 98–102.
- (24) Hong, M. *J. Magn. Reson.* **1999**, *139*, 389–401.
- (25) Bayro, M. J.; Maly, T.; Birkett, N. R.; Dobson, C. M.; Griffin, R. G. *Angew. Chem., Int. Ed.* **2009**, *48*, 5708–5710.
- (26) Nieuwkoop, A. J.; Wylie, B. J.; Franks, W. T.; Shah, G. J.; Rienstra, C. M. *J. Chem. Phys.* **2009**, *131*, 8.
- (27) Bayro, M. J.; Maly, T.; Birkett, N. R.; MacPhee, C. E.; Dobson, C. M.; Griffin, R. G. *Biochemistry* **2010**, *49*, 7474–7484.
- (28) Saper, M. A.; Bjorkman, P. J.; Wiley, D. C. *J. Mol. Biol.* **1991**, *219*, 277–319.
- (29) Petterson, E. F.; Goddard, T. D.; Huang, C. C.; Couch, G. S.; Greenblatt, D. M.; Meng, E. C.; Ferrin, T. E. *J. Comput. Chem.* **2004**, *25*, 1605–1612.
- (30) Debelouchina, G. T.; Bayro, M. J.; van der Wel, P. C. A.; Caporini, M. A.; Barnes, A. B.; Rosay, M.; Maas, W. E.; Griffin, R. G. *Phys. Chem. Chem. Phys.* **2010**, *12*, 5911–5919.
- (31) Trinh, C. H.; Smith, D. P.; Kalverda, A. P.; Phillips, S. E. V.; Radford, S. E. *Proc. Natl. Acad. Sci. U.S.A.* **2002**, *99*, 9771–9776.
- (32) Iwata, K.; Matsuura, T.; Sakurai, K.; Nakagawa, A.; Goto, Y. *J. Biochem.* **2007**, *142*, 413–419.
- (33) Verdone, G.; Corazza, A.; Viglino, P.; Pettirossi, F.; Giorgetti, S.; Mangione, P.; Andreola, A.; Stoppini, M.; Bellotti, V.; Esposito, G. *Protein Sci.* **2002**, *11*, 487–499.
- (34) Kardos, J.; Okuno, D.; Kawai, T.; Hagihara, Y.; Yumoto, N.; Kitagawa, T.; Zavodszky, P.; Naiki, H.; Goto, Y. *Biochim. Biophys. Acta* **2005**, *1753*, 108–120.
- (35) Fabian, H.; Gast, K.; Laue, M.; Misselwitz, R.; Uchanska-Ziegler, B.; Ziegler, A.; Naumann, D. *Biochemistry* **2008**, *47*, 6895–6906.

JA107987F